J. Fluid Mech. (1988), *vol.* 187, *pp.* 301–318
Printed in Great Britain

Settling behaviour of heavy and buoyant particles from a suspension in an inclined channel

By DAVID HIN-SUM LAW,
Alberta Research Council, Energy Resources Division. Oil Sands Research Department, Edmonton, Alberta, Canada

ROBERT S. MACTAGGART, K. NANDAKUMAR AND JACOB H. MASLIYAH
Department of Chemical Engineering, University of Alberta, Edmonton, Alberta, T6G 2G6, Canada

(Received 24 July 1986 and in revised form 20 July 1987)

Settling characteristics of bidisperse suspensions containing light and heavy particles in inclined channels have been studied both experimentally and theoretically. The suspension is relatively dilute with a total volume fraction of no more than 0.16. In this dilute range the flow-visualization experiments indicate the formation of distinct zones with clear interfaces between them. There is no evidence of lateral segregation of particles. The convection currents formed near an inclined boundary are transferred to different zones depending on the relative concentration of the two species. Based on the flow-visualization experiments, the well known Ponder–Nakamura–Kuroda (PNK) model has been adopted to predict the settling characteristics of bidisperse suspensions.

1. Introduction

Separation of light and heavy particles from a suspension with the aid of gravity is an industrially important process found in many mineral-processing operations. It also has evoked a strong interest from a theoretical point of view as some of the experimentally observed phenomena still remain unexplained. Two mechanisms have been identified in recent years as possible candidates for improving the performance of gravity separation vessels. The first one, termed the *Boycott effect* (Boycott 1920), has been observed when settling occurs near an inclined boundary. The second one, termed the *fingering phenomenon* (Whitmore 1955), has been observed when settling of two different species occurs above a certain threshold concentration of particles. Each of these two mechanisms has been studied by a number of investigators. In the present work we examine the Boycott effect as applied to the separation of light and heavy particles in inclined channels, i.e. the results are restricted to low-concentration regions where the fingering phenomenon is absent.

The Boycott effect has been studied extensively. A good summary of recent developments has been presented by Davis & Acrivos (1985). The earliest model explaining this phenomenon, based on kinematic and geometrical arguments, was developed by Ponder (1925) and Nakamura & Kuroda (1937). Subsequent studies on the separation of single species suspensions in inclined channels can be organized into two groups. The first group, by Kinosita (1949), Pearce (1962), Graham & Lama

(1963), Oliver & Jenson (1964), Vohra & Ghosh (1971) and Zahavi & Rubin (1975), depend on some empirically modified form of the PNK theory to explain their experimental findings. The second group, by Hill, Rothfus & Li (1977), Acrivos & Herbolzheimer (1979), Herbolzheimer & Acrivos (1981), Schneider (1982), Davis, Herbolzheimer & Acrivos (1982), Herbolzheimer (1983), Schaflinger (1985*a*, *b*), have taken a more fundamental approach to modelling based on the ensemble-averaged flow equations. Acrivos & Herbolzheimer (1979) were the first to identify the precise conditions under which the Ponder–Nakamura–Kuroda (PNK) theory is a valid representation of the settling process near an inclined boundary. Recognizing flow instability as one of the causes of departure from the PNK model, Herbolzheimer (1983) has presented a stability analysis for settling near an inclined wall. The effect of polydisperse suspensions, when all species are heavier than the fluid, has been studied by Davis *et al.* (1982) and by Schaflinger (1985*b*). Schaflinger has shown that particles in polydisperse suspensions under moderately high Reynolds number can also become resuspended, resulting in departure from the PNK model.

Sedimentation of particles of non-uniform size and/or density (polydisperse systems) in vertical containers has been studied quite extensively. Two classes of sedimentation process have been identified for polydisperse systems. The first one is for regions of low concentration where no lateral heterogeneities develop. Several distinct zones form and clearly identifiable interfaces separating the zones exist. Such cases can be modelled adequately with the aid of material balances written across the discontinuous interfaces or 'shocks' separating the various zones. The drift-flux or slip-velocity information is still needed. Application of such data, measured under monodispersed conditions, to polydisperse systems has been found to be adequate in most cases. Such systems have been studied by Richardson & Meikle (1961), Smith (1966), Lockett & Al-Habbooby (1973, 1974), Lockett & Bassoon (1979), Mirza & Richardson (1979), Masliyah (1979), Batchelor & Wen (1982), Greenspan & Ungarish (1982), Selim, Kothari & Turian (1983), Patwardhan & Tien (1985). While most of these studies have used polydisperse suspensions settling in the same direction (all heavy particles), the approach can be readily applied to heavy- and light-particle mixtures as well (Law *et al.* 1987). Separation of bidisperse systems containing light and heavy particles in inclined channels, however, has not been studied. This is the subject of the present work. We begin with some flow-visualization experiments to identify the patterns of separation and then present an extension of the PNK approach to model such bidisperse systems. Experimentally measured settling rates are then compared with the predictions from the PNK model.

The second class of separation for polydisperse systems is for regions of high concentration where lateral heterogeneities develop spontaneously from an initially homogeneous mixture. Separation of such systems in vertical containers has been studied quite extensively since the work of Whitmore (1955). Flow-visualization results confirming the spontaneous formation of fingers have been presented by Weiland, Fessas & Ramarao (1984). Settling-rate measurements and generalized correlations have been presented by Weiland & McPherson (1979) and Fessas & Weiland (1981, 1982, 1984). More recent experiments by Batchelor & Janse van Rensburg (1986) over a wider range of parameters indicate that these structures need not always be columnar or finger-like. They have also presented the first rational explanation for the formation of such organized structures. They are believed to be due to the instability of the bidisperse suspension under certain conditions and the growth of a bidisperse form of the concentration wave well known in monodisperse systems. Particle motions caused only by gravity and hydrodynamic interaction are

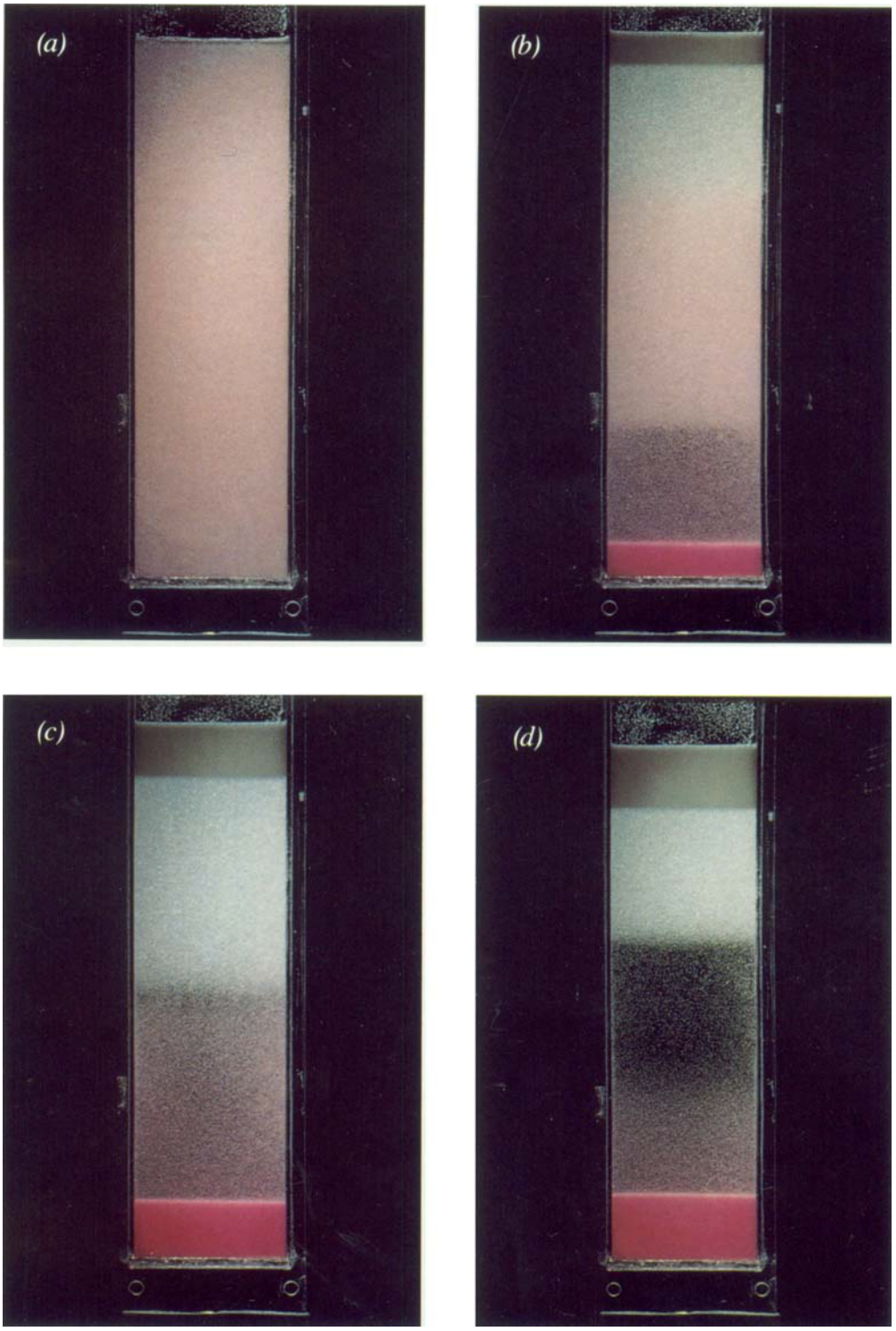

FIGURE 1. Settling behaviour for the vertical case with concentrations of 0.08 light and 0.08 heavy particles at (*a*) 0 s; (*b*) 100 s; (*c*) 190 s; (*d*) 200 s.

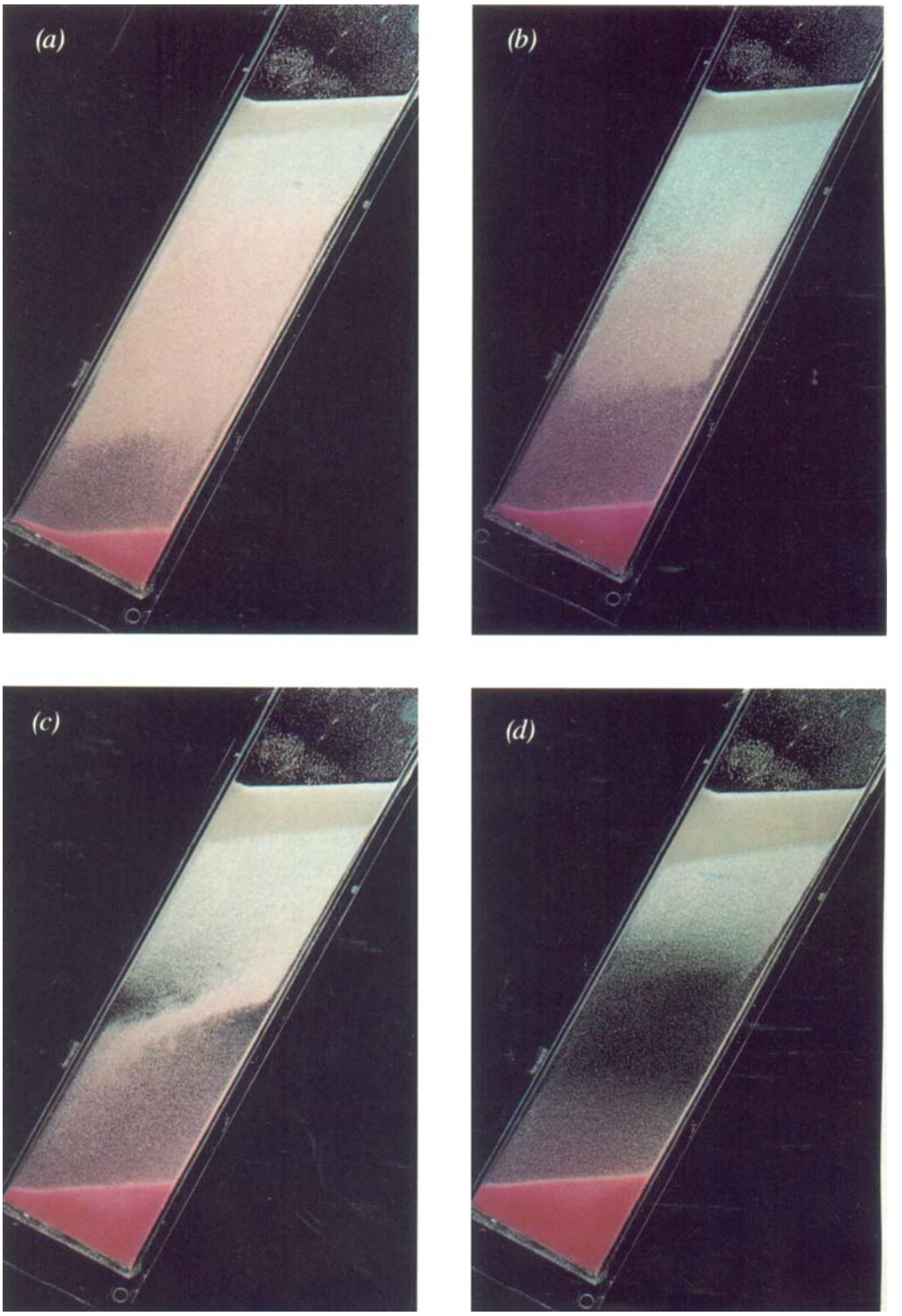

FIGURE 2. Settling behaviour at an inclination of 30° from vertical with concentrations of 0.08 light and 0.08 heavy particles at (*a*) 40 s; (*b*) 60 s; (*c*) 85 s; (*d*) 120 s.

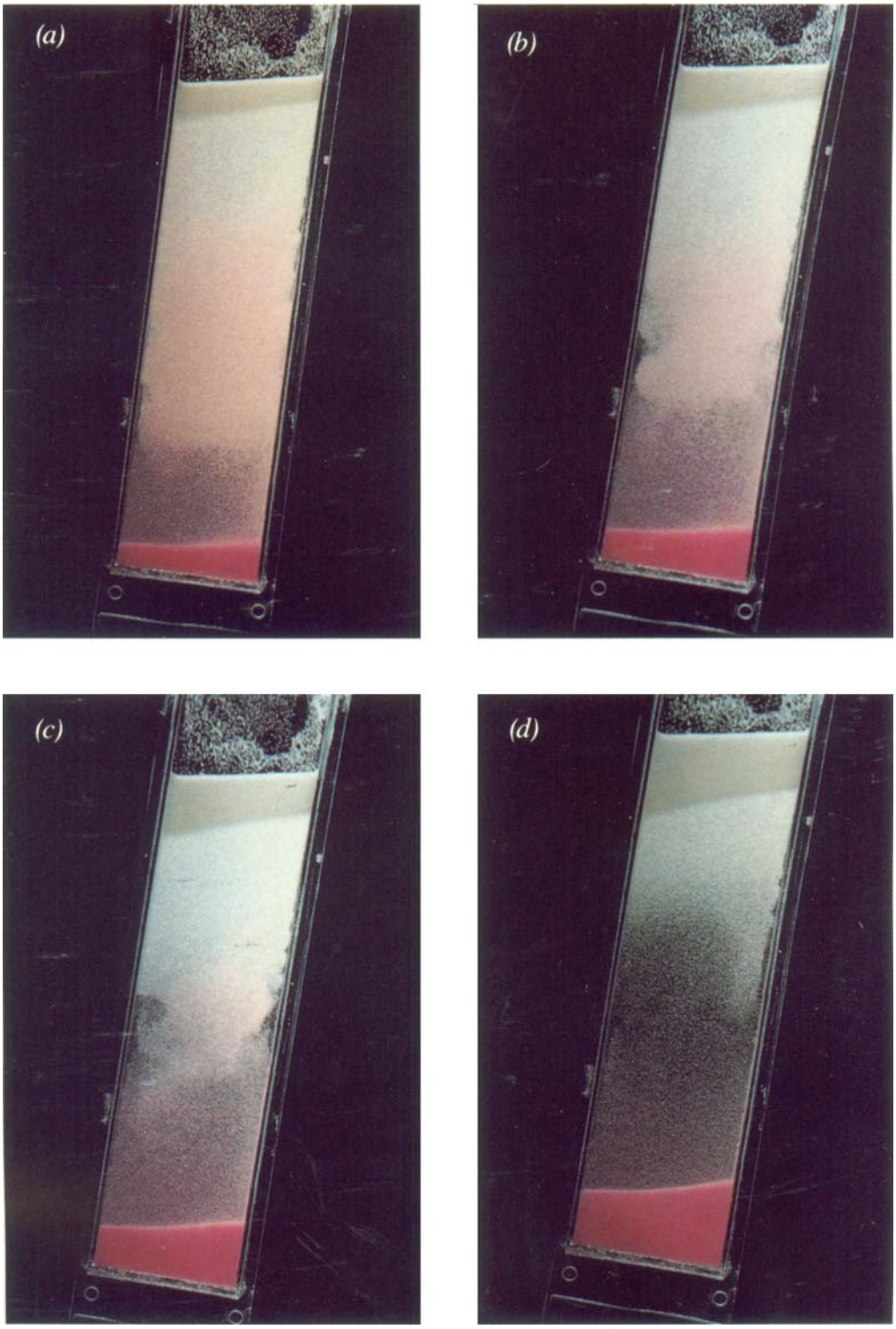

FIGURE 3. Settling behaviour at an inclination of 10° from vertical with concentrations of 0.08 light and 0.08 heavy particles at (*a*) 75 s; (*b*) 105 s; (*c*) 135 s; (*d*) 185 s.

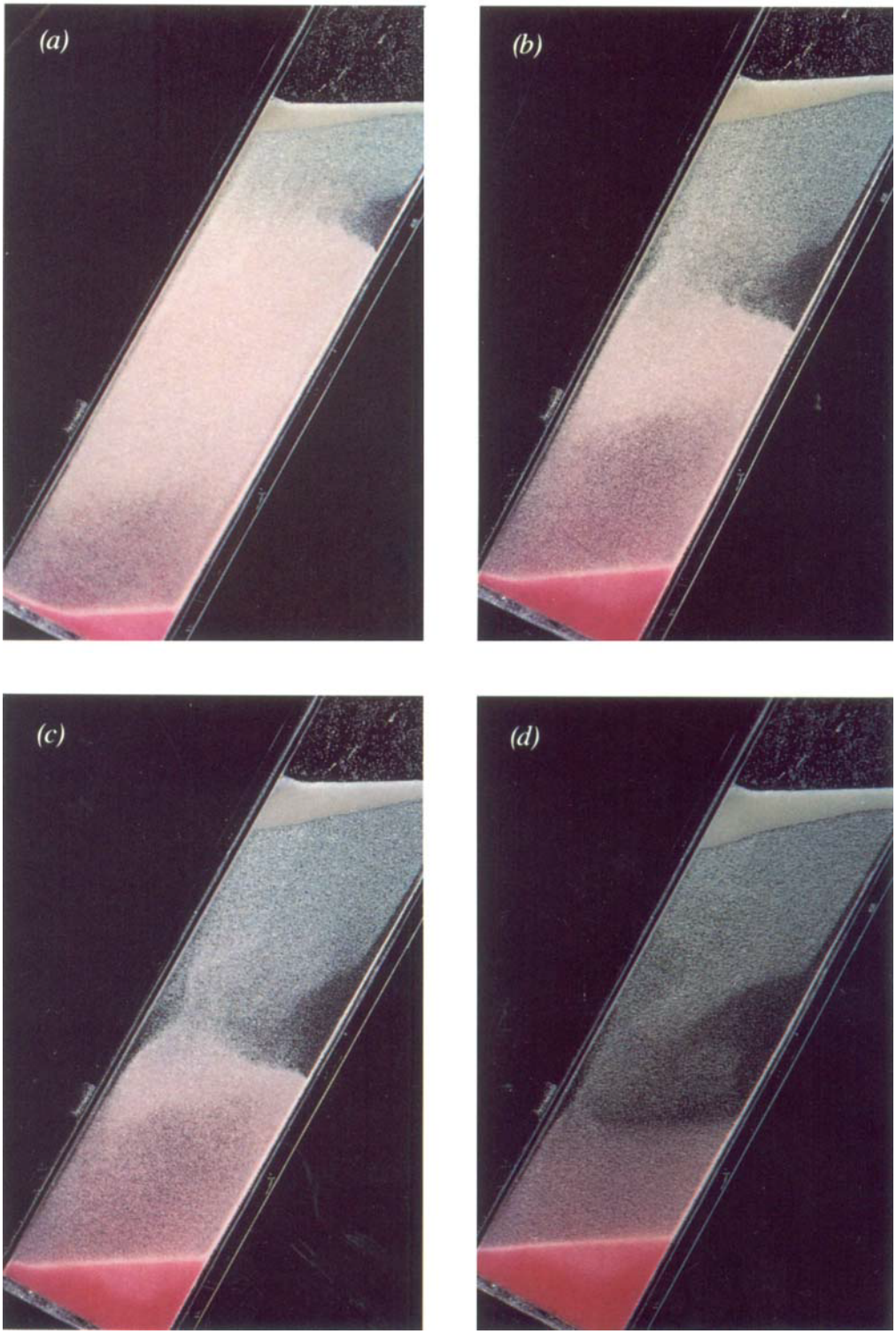

FIGURE 4. Settling behaviour at an inclination of 30° from vertical with concentrations of 0.04 light and 0.08 heavy particles at (*a*) 35 s; (*b*) 65 s; (*c*) 80 s; (*d*) 105 s.

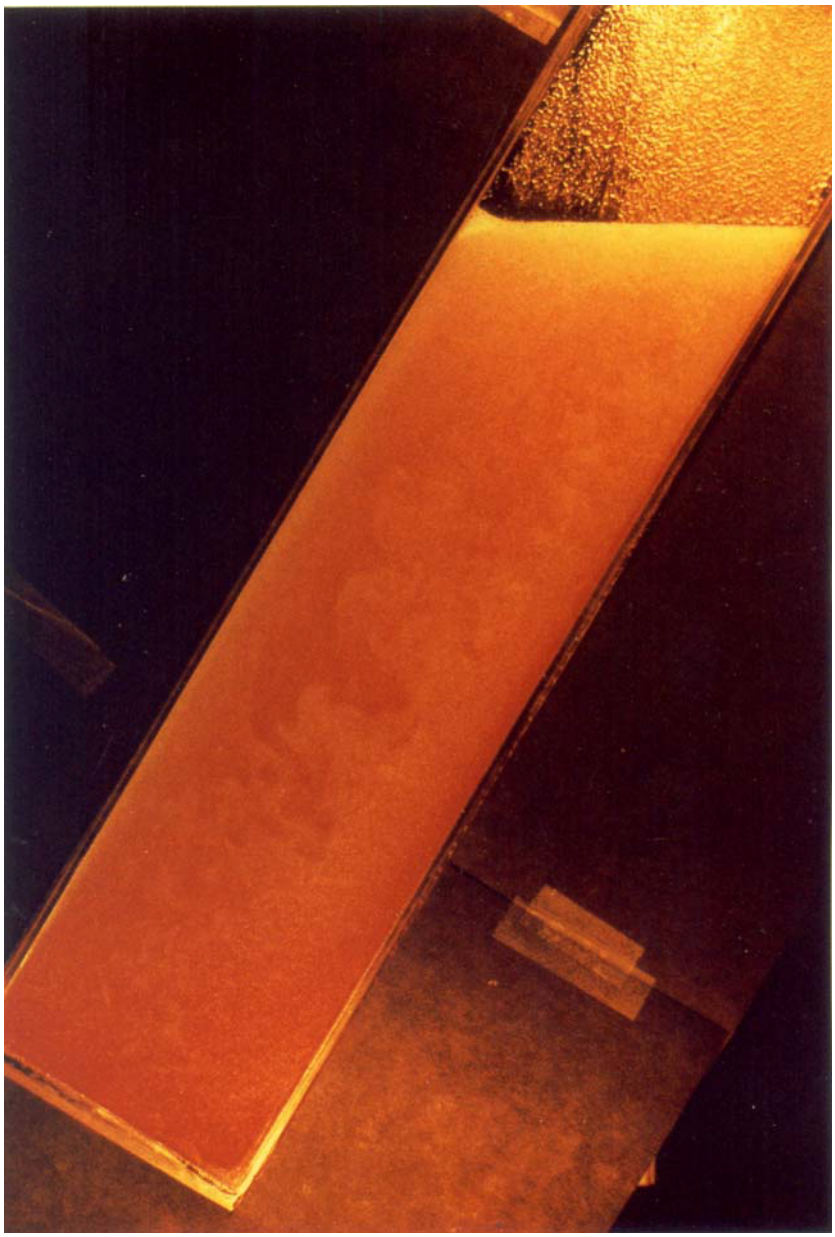

FIGURE 5. Finger formation at an inclination of 30° from vertical with concentrations of 0.2 light and 0.15 heavy particles at 10 s.

believed to be the cause of this phenomenon. Cox (1987) has developed a similar theory including the effect of physical contact between particles. Separation of bidisperse systems containing light and heavy particles in inclined channels, where the fingering effect coupled with the Boycott effect are present, has not been studied to date. Flow-visualization results and settling-rate measurements for such systems will be presented elsewhere.

2. Flow-visualization experiments

Batch settling experiments were performed in a rectangular Plexiglas container 37 cm in height and 8 cm × 0.5 cm in cross-section. The bidisperse suspensions were made of uniform-sized particles of polystyrene (PS, light) and polymethyl methacrylate (PMMA, heavy) dispersed in a sodium chloride solution. The density of the solution was adjusted to be midway between the densities of the two particles by altering the salt concentration. Approximately 0.05 wt % of Triton X-100 was added to the suspension to prevent flocculation. The properties of the particles and the liquid are presented in table 1.

The heavy particles (PMMA) were dyed with Rhodamine B to visually distinguish them from the white, light (PS) particles. The settling behaviour was observed for three sets of volume fractions of particles (0.08 PS–0.08 PMMA, 0.04 PS–0.08 PMMA, and 0.08 PS–0.04 PMMA) at various angles of inclination from the vertical. For each suspension the initial vertical height was kept constant at 28.3 cm. Patterns of settling behaviour can be broadly grouped into three categories: (i) low-concentration, symmetric, (ii) low-concentration asymmetric and (iii) high-concentration. Each one is described below.

Low-concentration, symmetric case

In the symmetric case the diameters and concentrations of the light and heavy particles are approximately equal and their densities are symmetrical with respect to the fluid. A time sequence of the settling behaviour for the symmetric case in the low-concentration region is shown in figures 1–3 at angles of inclination of 0°, 30° and 10° from the vertical, respectively. For the vertical case, initially, as shown in figure 1*a* at $t = 0$ s (Plate 1), the suspension is uniform, having a volume fraction of 0.08 of each species. Immediately thereafter (figure 1*b*) and until disengagement of the two species (figure 1*c*), i.e. over the time interval of $0 < t < t_c$, five distinct zones with sharp interfaces between them can be observed. From top to bottom these zones are light (PS)-sediment, light (PS)-suspension, bidisperse (PS and PMMA)-suspension, heavy (PMMA)-suspension and heavy (PMMA)-sediment zones. The middle interfaces are observed to rise or fall at uniform velocities. After disengagement ($t_c < t < t_s$) the two species continue to settle independently of each other, leaving behind a clear-fluid zone in between them (figure 1*d*).

Figure 2 (Plate 2) shows a similar set of photographs for the same suspension at an inclination of 30° from the vertical. An idealized sketch of the settling process is given in figure 6(*a*–*c*). During the partial segregation period (figure 2*a*–*c*, $0 < t < t_c$), five distinct zones are observed for this case also and the interfaces separating the zones are nearly horizontal. In addition, convection currents are also observed. Near the top of the upward-facing plate, a clear-fluid zone is left behind by the rising light (PS)-suspension zone. Since its density is higher than that of the light-suspension zone, this fluid slides down and mixes with the heavy (PMMA)-suspension zone formed near the middle of the upward-facing plate. Thus the clear fluid produced

	Particle species		Suspending fluid
Property	PS	PMMA	Salt solution
ρ (g/cm^3)	1.050	1.186	1.120
d (cm)	0.0241	0.0237	
μ (g/cm s)			0.0141

TABLE 1. Properties of particle species and suspending fluid

below the light (PS)-suspension zone is convected into the heavy (PMMA)-suspension zone, i.e. just below the rising light-particle interface (viz. interface C in figure 6*b*). The heavy (PMMA)-sediment formed in the lower part of the upward-facing plate slides down to join the sediment at the bottom. A similar process occurs beneath the downward-facing plate. The clear fluid produced by the falling heavy (PMMA)-suspension zone is convected to the light (PS)-suspension zone, i.e. just above the falling heavy-particle interface (viz. interface B in figure 6*b*). After disengagement ($t_c < t < t_s$) the two species continue to settle independently of each other, as in the case of any monodisperse settling (figure 2*d*).

The stability analysis by Herbolzheimer (1983) for monodisperse systems indicates that the waves formed in the convection zone grow at the maximum rate for an angle of about 10° from the vertical. A similar process occurs for the bidisperse suspensions also, as indicated in figure 3 (Plate 3). The waves formed at both the plates cause significant distortion of the interface. When the interfaces are not sharp, the height *vs.* time results presented later correspond to those measured along the centreline of the container.

Low-concentration, asymmetric case

Using the same fluid–particle system as in the previous case, a set of experiments was performed using unequal concentrations of particles. The volume fractions of the light (PS) and heavy (PMMA) particles were changed to 0.04 and 0.08 respectively. Figure 4 (Plate 4) shows the settling behaviour for this case at an angle of 30°. Once again five distinct zones begin to develop. However there is one major difference from the previous case. The clear fluid produced by the rising light (PS)-suspension zone near the top of the upward-facing plate is not transferred to the heavy (PMMA)-suspension zone as in the previous case, but is transferred to a region above the bidisperse-suspension zone (figure 4*a*, *b*). A sketch of this is shown in figure 6(*d*). This behaviour is to be expected for the following reasons. Since there are more heavy particles in the suspension, the suspension density (1.122) is higher than that of the clear-fluid density (1.120). Also, since the Reynolds number is small the inertia is not sufficient to move the clear fluid to the heavy-suspension zone. Notice that in figure 4(*b*, *c*) light (PS) particles are still present in the bidisperse zone (between interfaces B and C) and settle to the light suspension zone via the upper part of the channel; hence the light-suspension interface is severely distorted at the time of disengagement. As there are more heavy particles, its interface continues to be nearly horizontal.

For any combination of initial particle concentrations in the bidisperse zone we can expect the above behaviour as long as the suspension density in the bidisperse zone is sufficiently higher than that of the pure fluid. When the suspension density is equal to that of the pure fluid we clearly see the pure fluid convected past the

bidisperse zone as sketched in figure 6(*e*). When the suspension density in only marginally higher than that of the fluid, it would be difficult to predict the destination of the pure-fluid stream produced near the upward-facing plate without a detailed solution of the dynamic equations.

A mirror image of this behaviour is observed when there are more light particles (i.e. 0.08 light – 0.04 heavy). For both of these cases wave formation was also observed for an inclination of 10°. The observations on the movement of the clear fluid were used in the adaptation of the PNK model for bidisperse suspensions.

High-concentration case

Figure 5 (Plate 5) shows the settling process during the partial segregation ($0 < t < t_c$) period of a bidisperse suspension with volume fractions of 0.15 light (PS) and 0.20 heavy (PMMA) particles at an inclination of 30° from the vertical. At these high solid concentrations, the fingering flow structure develops in the bidisperse zone. The convection pattern near the inclined boundary is similar to that observed for the low-concentration symmetric case. Clear fluid appears below the rising light (PS)-suspension zone near the top of the upward-facing plate and is transferred to the heavy (PMMA)-suspension zone. Similarly the clear fluid produced above the falling heavy (PMMA)-suspension zone near the bottom of the downward-facing plate is transferred to the light (PS)-suspension zone.

3. Model development

The schematic diagrams shown in figure 6 illustrate the idealizations used in the adaptation of the PNK model for the present case. First, when a rectangular container is tilted at an angle θ from the vertical, its shape (solid lines in figure 6*a*) at the bottom is approximated by a parallelogram (dashed lines in figure 6*a*) such that the sediment volume is equalized. This removes the mathematical singularity of infinite growth rate of sediment at the corner, without introducing a significant error in the model. Next, the interfaces separating the various zones are assumed to be horizontal. Figure 6(*b*, *c*) shows the typical interface position before and after disengagement of the two species. Figure 6(*d*–*f*) is based on the flow-visualization experiments described earlier. They illustrate the zones to which the clear fluid and sediments are transferred by convection, as used in the PNK model. In the following, all velocities are considered positive in the gravitational direction. ϕ denotes the volume fraction of solids. The first subscript l or h denotes the light or heavy particles and the second subscript m, b or s denotes quantities in the monodisperse-suspension, bidisperse-suspension and the sediment zones respectively. Velocities in the sediment zone refer to the sediment interface velocities. The solids concentrations are assumed to be spatially uniform in each zone at any given time and their values in the bidisperse zone are also assumed to remain constant with time. However, the concentrations in the monodispersed zones (viz. ϕ_{lm} between planes A and B and ϕ_{hm} between planes C and D of figure 6*e*) will change with time until the disengagement of the two phases, because pure-fluid streams are being added to these zones. These zones are assumed to be spatially homogeneous in the model and this appears to be adequate in predicting the settling rates at least at these low concentrations.

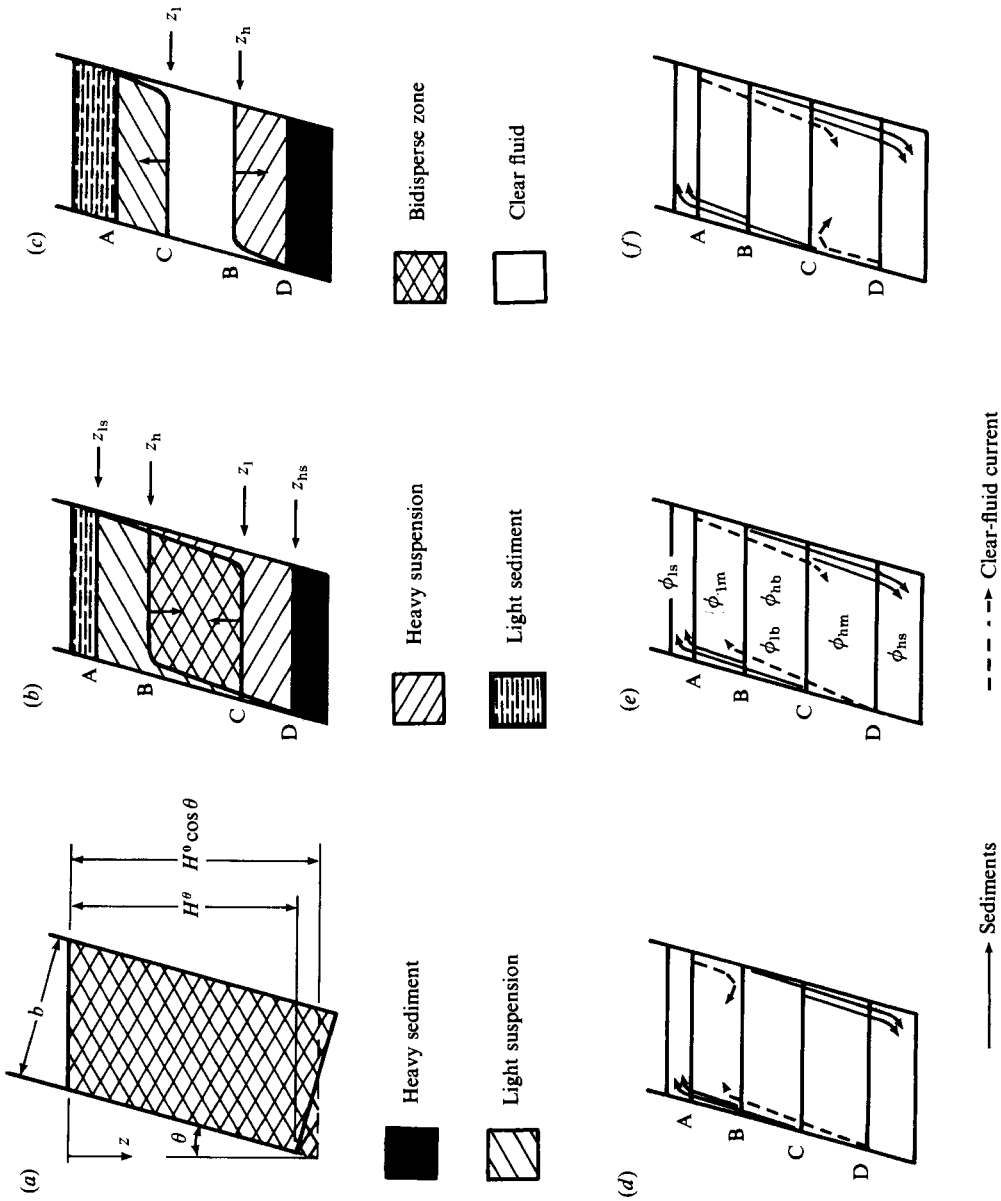

FIGURE 6. Schematic of settling behaviour for the PNK model. (*a–c*) Time sequence of settling behaviour: (*a*) $t = 0$; (*b*) $0 < t < t_c$; (*c*) $t_c < t < t_s$. (*d–f*) Settling behaviour during particle segregation ($0 < t < t_c$) at different concentrations: (*d*) 0.04 PS–0.08 PMMA; (*e*) 0.08 PS–0.08 PMMA; (*f*) 0.08 PS–0.04 PMMA.

3.1. *Review of PNK model for monodisperse systems*

Using the monodisperse light-particle system as an example, the PNK model, including the effect of sediment growth rate, is given by the following two equations for the two interfaces z_l and z_{ls}:

$$\frac{dz_l}{dt} = u_{lm}\left[1+\frac{z_l - z_{ls}}{b}\sin\theta\right], \tag{1}$$

$$\frac{dz_{ls}}{dt} = u_{ls}\left[1+\frac{z_l - z_{ls}}{b}\sin\theta\right]. \tag{2}$$

For $\theta = 0$, i.e. when the container is vertical, u_{lm} in (1) represents the interface velocity of a monodisperse system having a concentration of ϕ_{lm} and is obtained from the experimentally measured flux plot. Similarly, u_{ls} in (2) represents the sediment interface velocity and is obtained from the continuity equation written across the sediment interface:

$$u_{ls} = \frac{\phi_{lm}}{\phi_{lm}-\phi_{ls}}u_{lm}. \tag{3}$$

As the downward direction is taken as positive, u_{lm} becomes negative and u_{ls} becomes positive. In (3), the concentration in the suspension ϕ_{lm} is assumed constant at its initial value and that in the sediment ϕ_{ls} was experimentally measured to be 0.55. Integrating (1) and (2) subject to the initial conditions, $z_l(t=0) = H^\circ\cos\theta$ and $z_{ls}(t=0) = 0$, we obtain the height of the two interfaces as a function of time:

$$z_l = H^\circ\cos\theta - \left[\frac{(\phi_{ls}-\phi_{lm})}{\phi_{ls}}\frac{b+H^\circ\cos\theta\sin\theta}{\sin\theta}\right]\left[1-\exp\left(\frac{\phi_{ls}}{\phi_{ls}-\phi_{lm}}\frac{\sin\theta}{b}u_{lm}t\right)\right], \tag{4}$$

$$z_{ls} = \frac{\phi_{lm}}{\phi_{ls}}\left[\frac{b+H^\circ\cos\theta\sin\theta}{\sin\theta}\right]\left[1-\exp\left(\frac{\phi_{ls}}{\phi_{ls}-\phi_{lm}}\frac{\sin\theta}{b}u_{lm}t\right)\right]. \tag{5}$$

By replacing the subscript l (for light particle) in the above equations by h (for heavy particle) and with suitable changes in the initial conditions a similar set of equations, valid for a monodispersed heavy particle system, can be obtained. These equations also describe the settling process after the disengagement of the two species in a bidisperse system (i.e. figure 6*c*).

3.2. *Bidisperse systems during the partial segregation period*

Symmetric case

The time sequence of settling behaviour is sketched in figure 6(*a–c*). The initial locations of the interfaces are

$$z_l(t=0) = H^\circ\cos\theta, \quad z_{ls}(t=0) = 0, \tag{6}$$

$$z_h(t=0) = 0, \quad z_{hs}(t=0) = H^\circ\cos\theta. \tag{7}$$

During the partial segregation period, the observed convection patterns are sketched in figure 6(*d–f*). In the PNK model these currents are assumed to reach their destinations instantaneously. Let us consider first the symmetric case sketched in figure 6(*e*). To track the light-suspension interface C (i.e. the height z_l) for example, consider the volume above this interface. Any material taken out of this volume (viz. clear fluid between A and B and heavy suspension between B and C produced close to the upward-facing plate) will enhance the upward movement of the interface C

while any material added into this volume (viz. clear fluid produced below the downward-facing plate between C and D) will impede the upward movement of interface C. Thus the interface velocity z_l is given by

$$\frac{dz_l}{dt} = u_{lb}\left[1+\frac{z_l-z_h}{b}\sin\theta\right]+\left[u_{lm}\frac{z_h-z_{ls}}{b}+u_{hm}\frac{z_{hs}-z_l}{b}\right]\sin\theta. \tag{8}$$

I II III IV

u_{lm} in (8) represents the interface velocity of a monodisperse system having a concentration of ϕ_{lm} and is positive. The first term on the right-hand side I refers to the vertical settling velocity of the light particles in the bidisperse-suspension zone. The second term II is the enhancement due to the material left behind by the rising light particles close to the upward-facing plate between planes B and C. Since this layer is very small in thickness the details regarding clarification obtained within this zone (i.e. heavy suspension or clear fluid?) cannot be resolved. Instead all the material in this zone is added to the heavy-suspension zone between planes C and D. The third term III is the enhancement due to the clear fluid produced between planes A and B. The last term IV models the slowdown in the velocity of z_l caused by the clear fluid produced between planes C and D.

Similar reasoning leads to the following equations for the three remaining interfaces:

$$\frac{dz_h}{dt} = u_{hb}\left[1+\frac{z_l-z_h}{b}\sin\theta\right]+\left[u_{lm}\frac{z_h-z_{ls}}{b}+u_{hm}\frac{z_{hs}-z_l}{b}\right]\sin\theta, \tag{9}$$

$$\frac{dz_{ls}}{dt} = u_{ls}\left[1+\frac{z_l-z_{ls}}{b}\sin\theta\right], \tag{10}$$

$$\frac{dz_{hs}}{dt} = u_{hs}\left[1+\frac{z_{hs}-z_h}{b}\sin\theta\right]. \tag{11}$$

u_{hs} in (11) represents the sediment interface velocity for heavy particles and is negative. In the above equations u_{lb} and u_{hb} are the settling velocities of the light (PS) and heavy (PMMA) particles in the bidisperse zone (i.e. between interfaces B and C). Since the concentrations in this zone, ϕ_{lb} and ϕ_{hb}, are assumed to be constant at their original value, these velocities can be obtained from any model for polydisperse settling in a vertical direction. Several such models have been proposed (Smith 1966; Lockett & Al-Habbooby 1973, 1974; Mirza & Richardson 1979; Masliyah 1979 etc.); but we use the latter:

$$u_{lb} = \frac{u^*_{lm}}{(1-\phi_{lb}-\phi_{hb})^2}\frac{\rho_l-\rho_b}{\rho_l-\rho_f}(1-\phi_{lb})-\frac{u^*_{hm}}{(1-\phi_{lb}-\phi_{hb})^2}\frac{\rho_h-\rho_b}{\rho_h-\rho_f}\phi_{hb}, \tag{12}$$

$$u_{hb} = \frac{u^*_{hm}}{(1-\phi_{lb}-\phi_{hb})^2}\frac{\rho_h-\rho_b}{\rho_h-\rho_f}(1-\phi_{hb})-\frac{u^*_{lm}}{(1-\phi_{lb}-\phi_{hb})^2}\frac{\rho_l-\rho_b}{\rho_l-\rho_f}\phi_{lb}, \tag{13}$$

where $\rho_b = \rho_l\phi_{lb}+\rho_h\phi_{hb}+\rho_f(1-\phi_{lb}-\phi_{hb})$. ρ_l and ρ_h represent the densities of the light and heavy particles, respectively, and ρ_f and ρ_b represent the densities of the fluid and the bidisperse suspension respectively. The velocities u^*_{lm} and u^*_{hm} in (12) and (13) can be evaluated from the drift-flux relations for monodisperse systems of light and heavy particles respectively having a total solids concentration of $(\phi_{lb}+\phi_{hb})$.

The other unknown quantities in (8)–(11) are the sediment velocities u_{ls} and u_{hs},

the particle velocities u_{lm} and u_{hm} in the monodisperse zones, and the concentrations ϕ_{lm} and ϕ_{hm} in the monodisperse zones, and the concentrations ϕ_{lm} and ϕ_{hm} on which the above velocities depend. Four additional equations can be obtained by writing the continuity equations across the moving interfaces and the remaining two equations are the experimentally obtained drift-flux expressions relating the velocities to concentrations. The continuity equations are

$$u_{ls} = \frac{\phi_{lm}}{\phi_{lm}-\phi_{ls}} u_{lm}, \tag{14}$$

$$u_{hs} = \frac{\phi_{hm}}{\phi_{hm}-\phi_{hs}} u_{hm}, \tag{15}$$

$$\phi_{lm} = \frac{(H^\circ \cos\theta - z_l + z_h)\,\phi_{lb} - z_{ls}\,\phi_{ls}}{z_h - z_{ls}}, \tag{16}$$

$$\phi_{hm} = \frac{[H^\circ \cos\theta - z_l + z_h]\,\phi_{hb} - [H^\circ \cos\theta - z_{hs}]\,\phi_{hs}}{z_{hs} - z_l}. \tag{17}$$

The experimentally measured velocity–concentration relationships were fitted by a polynomial approximation as suggested by Shannon, Stroupe & Tory (1963) and Shannon *et al.* (1964):

$$u_{jm} = \sum_{i=0}^{4} A_{ij}\,\phi_{jm}^{i} \quad (j = l, h). \tag{18}$$

The least-squares estimate of the constants A_{ij} are given in table 2. The simultaneous numerical solution of the four differential equations (8)–(11) and the six algebraic equations (14)–(18) provide the settling behaviour until disengagement of the two species.

Asymmetric case

For a bidisperse suspension with volume fractions of 0.04 light (PS) and 0.08 heavy (PMMA), the convection patterns are given in figure 6(*d*). The only difference is that clear fluid accumulates above plane B because its density is lower than that of the suspension ρ_b. Equations (8) and (9) must be replaced by the following:

$$\frac{dz_l}{dt} = u_{lb}\left[1 + \frac{z_l - z_h}{b}\sin\theta\right] + \left[u_{hm}\frac{z_{hs} - z_l}{b}\right]\sin\theta, \tag{19}$$

$$\frac{dz_h}{dt} = u_{hb}\left[1 + \frac{z_l - z_h}{b}\sin\theta\right] + \left[u_{hm}\frac{z_{hs} - z_l}{b}\right]\sin\theta. \tag{20}$$

Note that the above equations would be correct even if the clear fluid produced above the upward-facing plate should mix with the bidisperse-suspension zone (i.e. between B and C), as it would affect z_l only if that stream crosses the interface C. Note however that the concentrations ϕ_{lb} and ϕ_{hb} in the bidisperse zone will change. Thus the above equations should be useful as long as $\rho_b > \rho_f$.

When $\rho_f > \rho_b$, the clear fluid accumulates below plane C as shown in figure 6(*f*). For this case (8) and (9) must be replaced by the following set:

$$\frac{dz_l}{dt} = u_{lb}\left[1 + \frac{z_l - z_h}{b}\sin\theta\right] + \left[u_{lm}\frac{z_h - z_{ls}}{b}\right]\sin\theta, \tag{21}$$

$$\frac{dz_h}{dt} = u_{hb}\left[1 + \frac{z_l - z_h}{b}\sin\theta\right] + \left[u_{lm}\frac{z_h - z_{ls}}{b}\right]\sin\theta. \tag{22}$$

Particle species	A_{0_j}	A_{1_j}	A_{2_j}	A_{3_j}	A_{4_j}
PS (j = l)	−0.1110	0.3802	0.3042	−2.5368	2.5368
PMMA (j = h)	0.1150	−0.4892	0.5547	0.2832	−0.6584

TABLE 2. Constants for power-series fit of experimental data in (18)

Time for complete separation

The model equations presented above are difficult to solve analytically without further approximations. An approximate solution will be compared with the full numerical solution in §4. However, a useful expression for the time of disengagement of the two species can be obtained quite readily. Subtracting (9) from (8) (or its equivalent replacement for the asymmetric cases) we obtain

$$\frac{\mathrm{d}(z_\mathrm{l}-z_\mathrm{h})}{\mathrm{d}t} = (u_{\mathrm{lb}}-u_{\mathrm{hb}})\left[1+\frac{z_\mathrm{l}-z_\mathrm{h}}{b}\sin\theta\right]. \tag{23}$$

This can be integrated subject to the initial condition $z_\mathrm{l}-z_\mathrm{h} = H^\circ\cos\theta$. The solution is

$$z_\mathrm{l}-z_\mathrm{h} = \frac{b+H^\circ\cos\theta\sin\theta}{\sin\theta}\exp\left[\frac{(u_{\mathrm{lb}}-u_{\mathrm{hb}})\sin\theta}{b}t\right]-\frac{b}{\sin\theta}. \tag{24}$$

Setting $z_\mathrm{l}-z_\mathrm{h} = 0$, the time for disengagement, t_c is obtained as

$$t_\mathrm{c} = \frac{b}{(u_{\mathrm{lb}}-u_{\mathrm{hb}})\sin\theta}\ln\left[\frac{b}{b+H^\circ\cos\theta\sin\theta}\right]. \tag{25}$$

Note that the above provides only the time of disengagement. The full model equations must be solved for the location of disengagement.

3.3. *Bidisperse systems after disengagement*

After disengagement of the two species, interfaces B and C move independently of each other and the results of §3.1 are valid as long as the initial time is replaced by t_c, the concentrations are those calculated at t_c from the model in §3.2 and the initial heights correspond to those at the time of disengagement. With these changes (4) and (5) become

$$z_\mathrm{l} = z_\mathrm{c}-\left[\frac{\phi_{\mathrm{ls}}-\phi_{\mathrm{lm}}(t_\mathrm{c})}{\phi_{\mathrm{ls}}}\frac{b+\{z_\mathrm{c}-z_{\mathrm{ls}}(t_\mathrm{c})\}\sin\theta}{\sin\theta}\right]\times\left[1-\exp\left(\frac{\phi_{\mathrm{ls}}}{\phi_{\mathrm{ls}}-\phi_{\mathrm{lm}}(t_\mathrm{c})}\frac{\sin\theta}{b}u_{\mathrm{lm}}(t-t_\mathrm{c})\right)\right], \tag{26}$$

$$z_{\mathrm{ls}} = z_{\mathrm{ls}}(t_\mathrm{c})+\left[\frac{\phi_{\mathrm{lm}}(t_\mathrm{c})}{\phi_{\mathrm{ls}}}\frac{b+\{z_\mathrm{c}-z_{\mathrm{ls}}(t_\mathrm{c})\}\sin\theta}{\sin\theta}\right]\times\left[1-\exp\left(\frac{\phi_{\mathrm{ls}}}{\phi_{\mathrm{ls}}-\phi_{\mathrm{lm}}(t_\mathrm{c})}\frac{\sin\theta}{b}u_{\mathrm{lm}}(t-t_\mathrm{c})\right)\right], \tag{27}$$

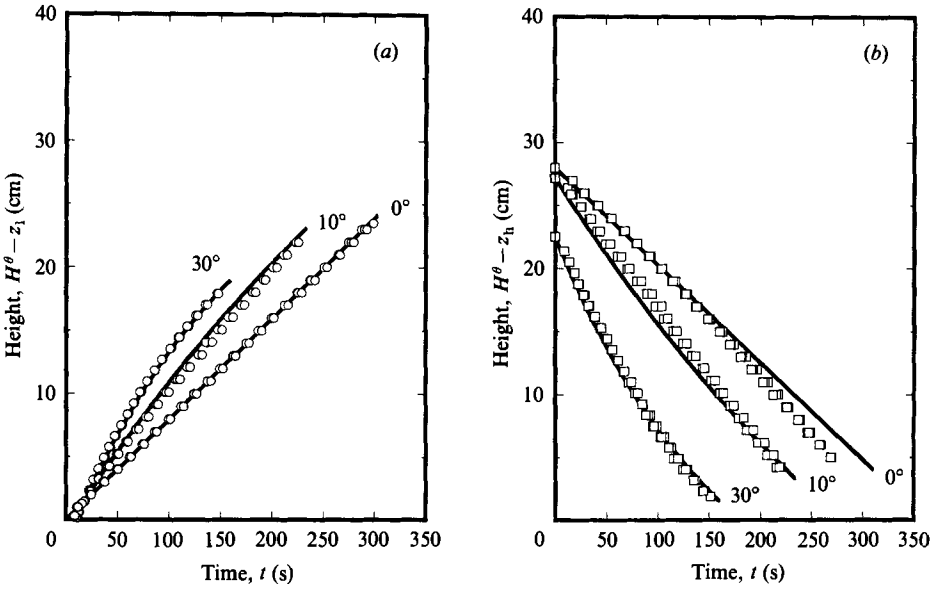

FIGURE 7. Comparison of experimental data (○, □) with the PNK model (——) for a monodisperse suspension: (*a*) 8% PS; (*b*) 8% PMMA.

$$z_h = z_c - \left[\frac{\phi_{hs}-\phi_{hm}(t_c)}{\phi_{hs}}\,\frac{b+\{z_{hs}(t_c)-z_c\}\sin\theta}{\sin\theta}\right] \times\left[1-\exp\left(\frac{-\phi_{hs}}{\phi_{hs}-\phi_{hm}(t_c)}\,\frac{\sin\theta}{b}\,u_{hm}(t-t_c)\right)\right], \quad (28)$$

$$z_{hs} = z_{hs}(t_c) + \left[\frac{\phi_{hm}(t_c)}{\phi_{hs}}\,\frac{b+\{z_{hs}(t_c)-z_c\}\sin\theta}{\sin\theta}\right] \times\left[1-\exp\left(\frac{-\phi_{hs}}{\phi_{hs}-\phi_{hm}(t_c)}\,\frac{\sin\theta}{b}\,u_{hm}(t-t_c)\right)\right]. \quad (29)$$

4. Results and discussion

Experimental data were obtained over the following range of parameters:

$$2.15 \leqslant H^\theta/b \leqslant 3.54, \quad 0° \leqslant \theta \leqslant 45°,$$
$$195 \leqslant Re_j \leqslant 353, \quad 7.3\times10^5 \leqslant \Lambda_j \leqslant 2.05\times10^6,$$
$$\phi_{jm} = 0.08, \quad b = 8\text{ cm} \quad (j = \text{l, h}),$$

where Re_j and Λ_j are respectively the Reynolds number and the ratio of Grashof number to Reynolds number. They are defined by Acrivos & Herbolzheimer (1979) as

$$Re_j = \frac{H^\theta d_j^2 \rho_f(\rho_j-\rho_f)g}{18\mu_f} \quad (j = \text{l, h}),$$

$$\Lambda_j = 18\left[\frac{H^\theta}{d_j}\right]^2 \phi_{jm} \quad (j = \text{l, h}),$$

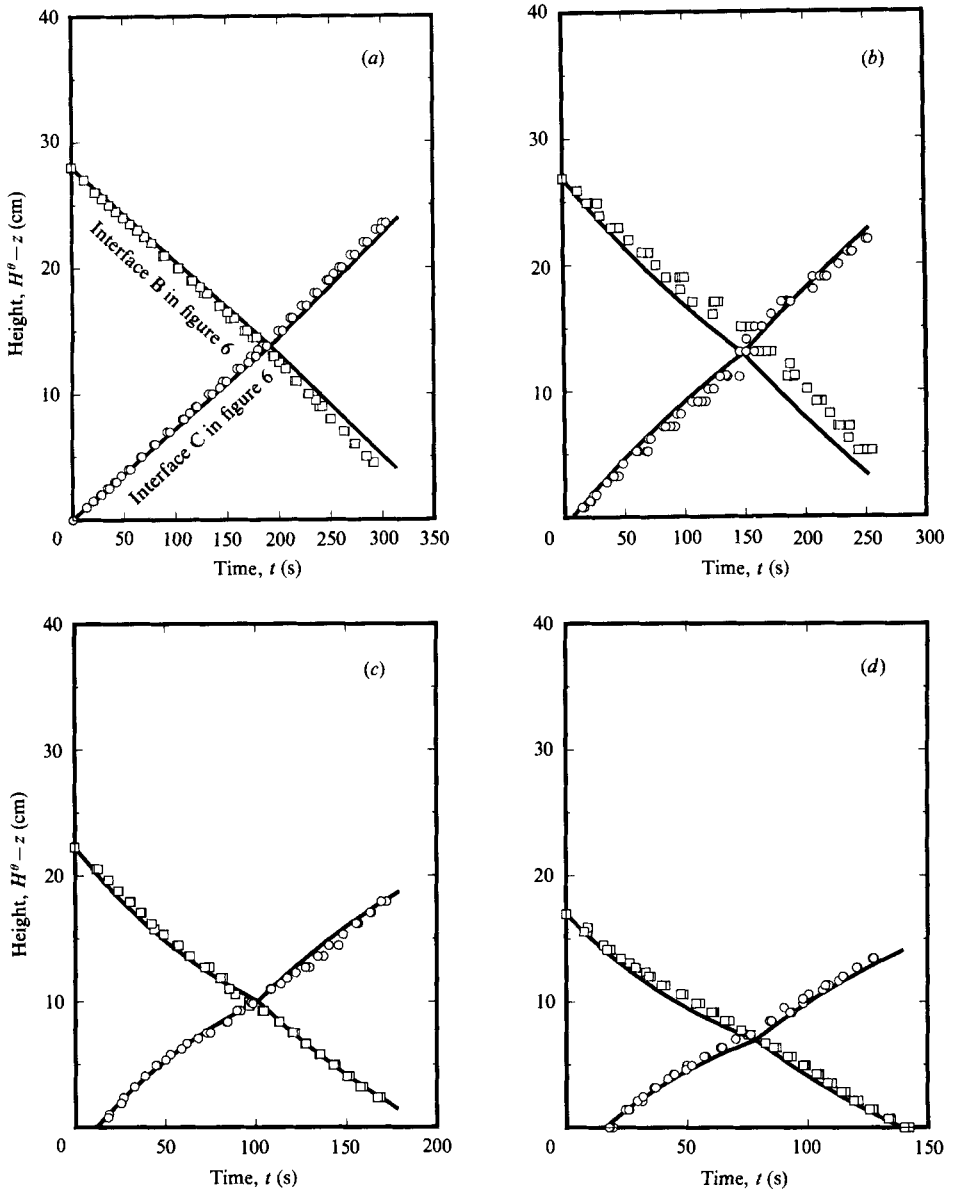

FIGURE 8. Comparison of experimental data with the modified PNK model for a symmetric bidisperse suspension with 0.08 light and 0.08 heavy particles, at (*a*) 0°, (*b*) 10°, (*c*) 30° and (*d*) 45° inclination from the vertical. ——, theory; ○, data for PS; □, data for PMMA.

where d_j are the particle diameters, ρ_f and μ_f are the density and viscosity of the fluid respectively. The PNK model for a monodisperse suspension is first compared with experimentally measured data in figure 7(*a*, *b*) for both the light (PS) and heavy (PMMA) particles at angles of 0°, 10° and 30°. There is a good agreement between the predictions from the model and the experiments. This is not surprising as Acrivos & Herbolzheimer (1979) and Herbolzheimer & Acrivos (1981) have shown that the PNK model is valid when $bA_j^{\frac{1}{3}}/H^\theta \gg 1$. For $bA_j^{\frac{1}{3}}/H^\theta \approx 40$, as in this study, the PNK model should be an adequate representation of the settling process.

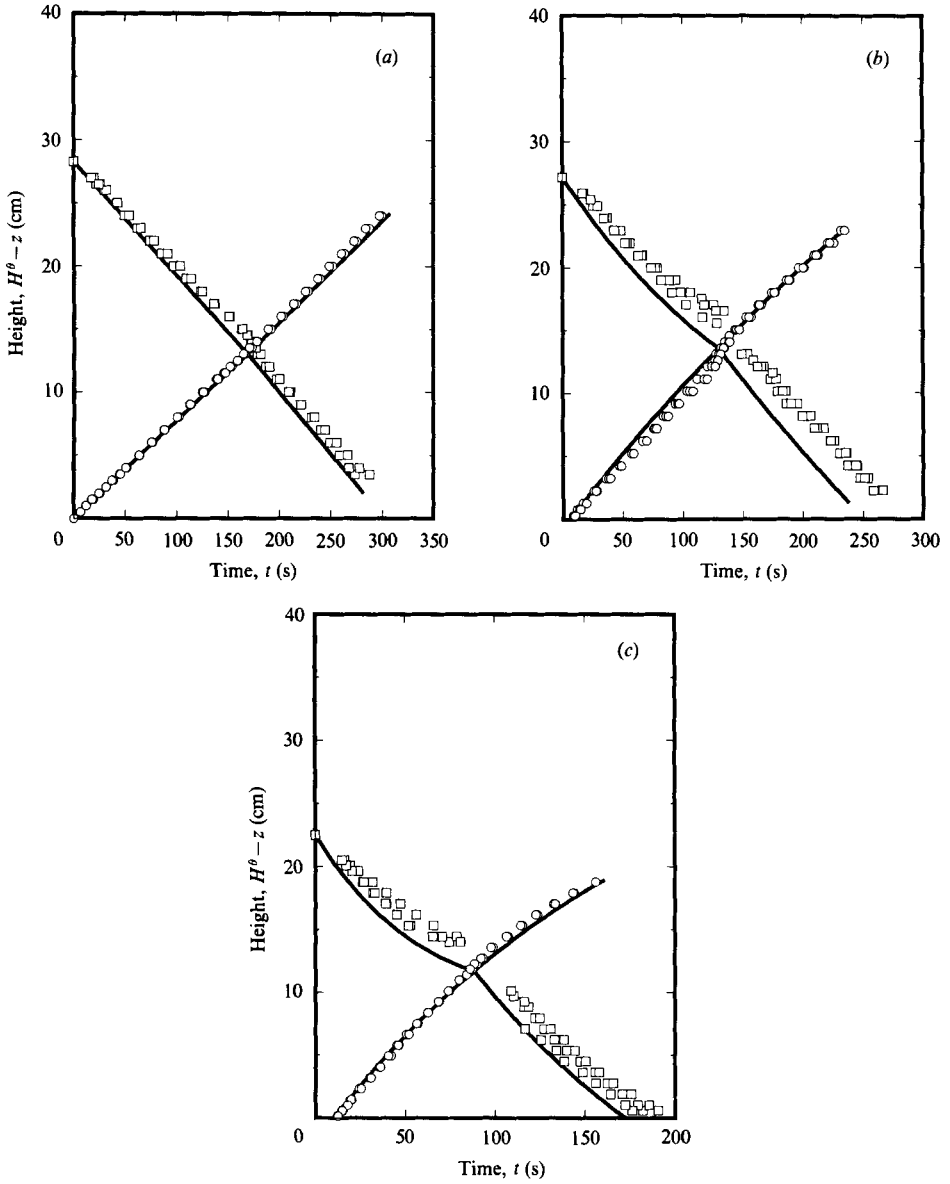

FIGURE 9. Comparison of experimental data with the modified PNK model for an asymmetric bidisperse suspension with 0.08 light and 0.04 heavy particles, at (*a*) 0°, (*b*) 10° and (*c*) 30° inclination from the vertical. Symbols as in figure 8.

The location of interfaces B and C of figure 6 as a function of time are shown in figures 8–10 for three different concentrations and at various angles of inclination. In all of these plots, the height H^θ refers to the distance from the reference point at the top of the channel to the bottom left corner of the channel as indicated in figure 6(*a*). Hence the rising interface C is shown only after it passes the lower left corner of the channel. In general the experimental data are reproducible and the data from several experimental runs are plotted on the same figure. The settling velocity is constant only for the vertical case in all these figures. Without the presence of inclined walls

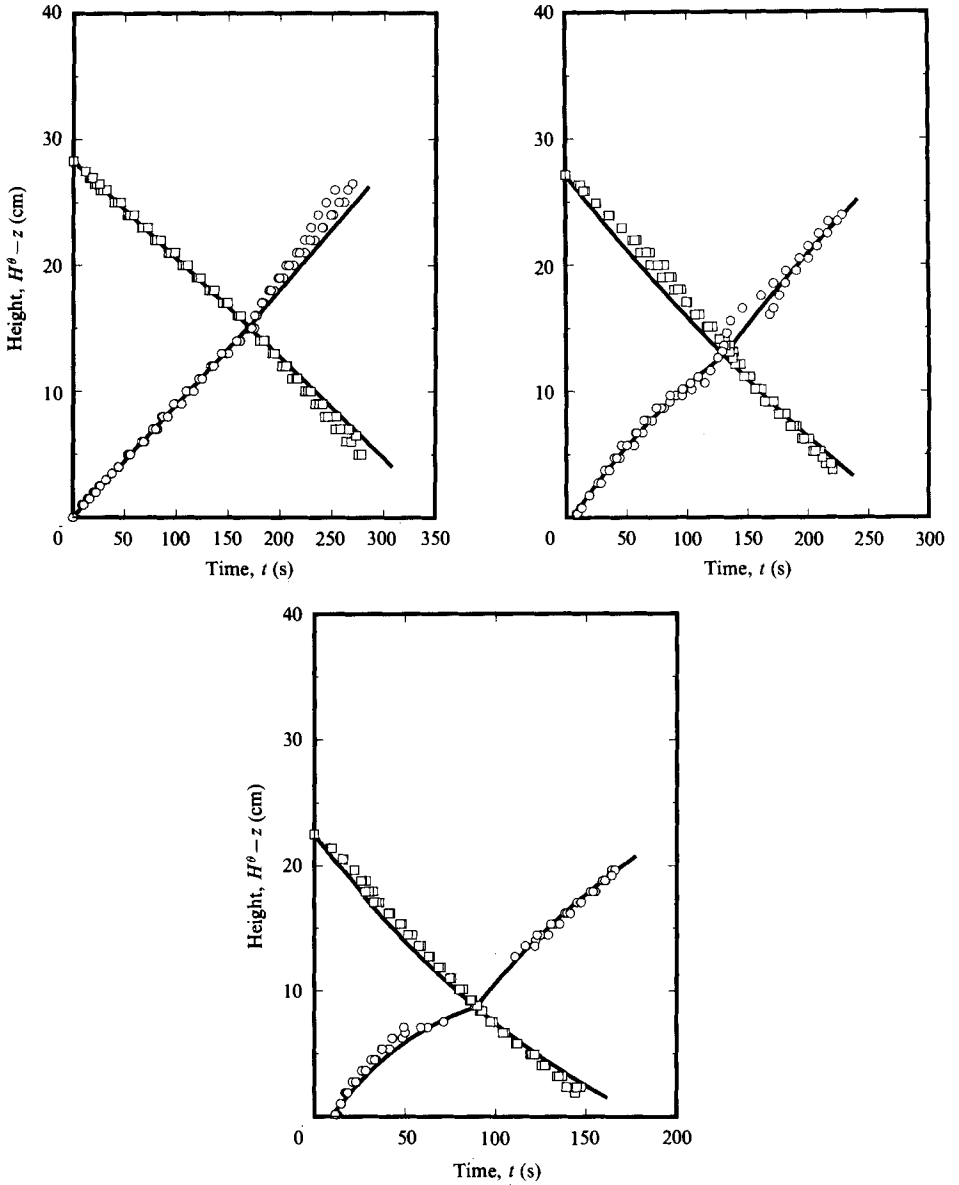

FIGURE 10. Comparison of experimental data with the modified PNK model for an asymmetric bidisperse suspension with 0.04 light and 0.08 heavy particles, at (*a*) 0°, (*b*) 10° and (*c*) 30° inclination from the vertical. Symbols as in figure 8.

the interfaces B and C fall and rise at uniform velocities u_{hb} and u_{lb} respectively. The PNK model reduces consistently to that of Smith (1966) for the vertical case. The agreement between the model prediction and experimental data is good, except when the inclination is 10° from the vertical. For the asymmetric cases (figures 9 and 10) the interface corresponding to the particles with the higher concentration could be tracked more accurately. The scatter is much wider for the other interface for reasons pointed out in the flow-visualization section. Note that the only experimental data

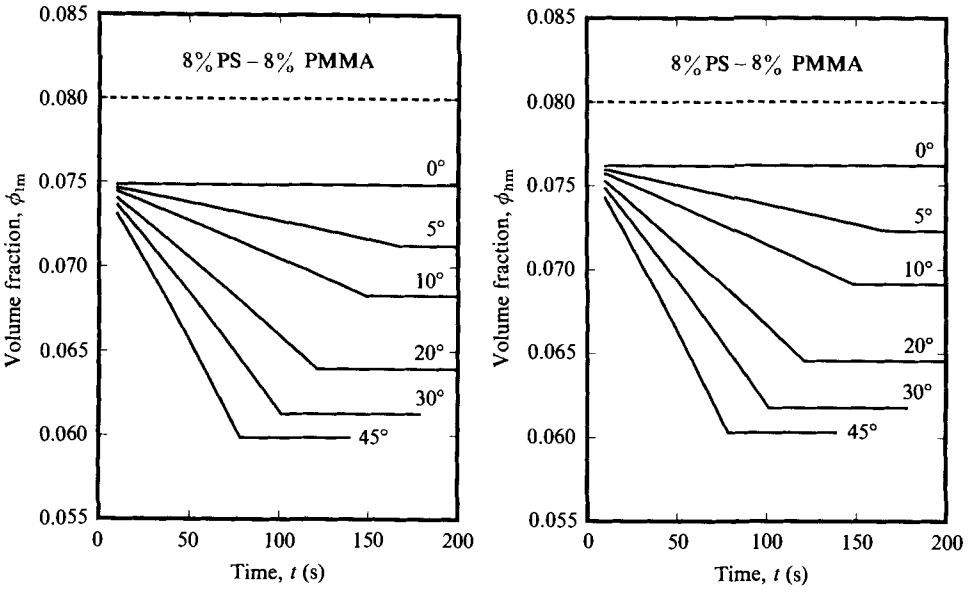

FIGURE 11. Variation of concentration with time in the monodisperse zones as predicted from the model, at various inclinations to the vertical.

required in the model is the drift-flux relationship which was measured for the vertical monodispersed systems and is given by (18). Additional effects such as the interaction between particles in the bidisperse zone as well as the boundary enhancement are modelled correctly without any additional experimental fit.

The concentration of particles in the monodispersed zones (between interfaces A and B for ϕ_{lm} and interfaces C and D for ϕ_{hm}) vary with time during the partial segregation period as shown in (16) and (17). The variation of these concentrations with time as calculated from the numerical model is shown in figure 11. The concentration decreases more rapidly at higher angles of inclination. But the change is not more than 25% of the initial value.

Approximate solutions

It is possible to obtain approximate analytical solutions to the model equations (8)–(18) subject to the following assumptions: (i) there is no accumulation of sediments, implying that $z_{ls} = 0$ and $z_{hs} = H^\circ \cos\theta$ are constants; and (ii) the concentrations in the monodispersed zones are constant, i.e. $\phi_{lm} = \phi_{lb}$ and $\phi_{hm} = \phi_{hb}$. Note that the difference $(z_l - z_h)$ given by (24) is valid without the above approximations. It can be used for example in (9) to eliminate z_l. The resulting equation for z_h is linear because of the assumption that u_{lm} can be calculated at the concentration $\phi_{lm} = \phi_{lb}$. The solutions obtained in this manner are shown in table 3. Although the concentrations ϕ_{lm} and ϕ_{lb} are assumed to be equal, the velocities u_{lm} and u_{lb} are not equal; u_{lm} is calculated directly from (18) while u_{lb} accounts for the particle interaction in the bidisperse zone through (12).

The height of disengagement can now be calculated from the approximate solution in table 3 together with (25). The experimentally observed height of disengagement is compared with the results calculated from the full numerical solution as well as the approximate analytical solution in table 4 for the symmetric-concentration case. The

	C_1	C_2	C_3	C_4
$\phi_{hb} \approx \phi_{lb}$	$\dfrac{u_{hm}}{u_{hm}-u_{lm}}$	$-C_1-\dfrac{u_{hb}-u_{hm}}{u_{hm}-u_{lm}+u_{lb}-u_{hb}}$	$-\dfrac{u_{hm}-u_{lm}}{b}\sin\theta$	$\dfrac{u_{hb}-u_{hm}}{u_{hm}-u_{lm}+u_{lb}-u_{hb}}$
$\phi_{hb} > \phi_{lb}$	1	$-\dfrac{u_{lb}}{u_{hm}+u_{lb}-u_{hb}}$	$-\dfrac{u_{hm}}{b}\sin\theta$	$\dfrac{u_{hb}-u_{hm}}{u_{hm}+u_{lb}-u_{hb}}$
$\phi_{hb} < \phi_{lb}$	0	$-\dfrac{u_{hb}}{-u_{lm}+u_{lb}-u_{hb}}$	$\dfrac{u_{lm}}{b}\sin\theta$	$\dfrac{u_{hb}}{-u_{lm}+u_{lb}-u_{hb}}$

TABLE 3. Analytical solutions

$$z_h = \frac{b+H^\circ \sin\theta\cos\theta}{\sin\theta}\left[C_1+C_2\exp(C_3 t)+C_4\exp\left(\frac{(u_{lb}-u_{hb})\sin\theta}{b}t\right)\right]$$

θ (deg)	Approximate analytical solution (cm)	Full numerical solution (cm)	Experimental data (cm)
5	13.434	13.441	13.69
10	12.956	12.956	13.09
20	11.677	11.678	11.60
30	10.039	10.033	9.86
45	7.004	6.999	7.42

TABLE 4. Comparison of height of disengagement

agreement is found to be very good. Similar comparisons for the asymmetric cases indicate an error of up to 7% in the approximate solution compared to the full numerical solution.

5. Conclusions

The settling behaviour of bidisperse suspensions containing light and heavy particles has been studied experimentally. Guided by the flow-visualization experiments, the PNK model has been adopted for bidisperse systems as well. The model predictions agree well with experimental results for a total solids volume fraction of 0.16. For higher concentrations an additional mechanism of fingering structure is observed.

This work was supported by a strategic grant from the National Science and Engineering Research Council of Canada.

REFERENCES

ACRIVOS, A. & HERBOLZHEIMER, E. 1979 Enhanced sedimentation in settling tanks with inclined walls. *J. Fluid Mech.* **92**, 435–457.

BATCHELOR, G. K. & JANSE VAN RENSBURG, R. W. 1986 Structure formation in bidisperse sedimentation. *J. Fluid Mech.* **166**, 379–407.

BATCHELOR, G. K. & WEN, C.-S. 1982 Sedimentation in a dilute polydisperse system of interacting spheres. Part 2. Numerical results. *J. Fluid Mech.* **124**, 495–528.

BOYCOTT, A. E. 1920 Sedimentation of blood corpuscles. *Nature* **104**, 532.

Cox, R. G. 1987 Sedimentation in bi-disperse suspensions. In *Proc. 11th Canadian Congress of Applied Mechanics. May 31–June 4, 1987, Edmonton, Canada.*

Davis, R. H. & Acrivos, A. 1985 Sedimentation of noncolloidal particles at low Reynolds numbers. *Ann. Rev. Fluid Mech.* **17**, 91–118.

Davis, R. H., Herbolzheimer, E. & Acrivos, A. 1982 The sedimentation of polydisperse suspensions in vessels having inclined walls. *Intl J. Multiphase Flow* **8**, 571–585.

Fessas, Y. P. & Weiland, R. H. 1981 Convective solids settling induced by a buoyant phase. *AIChE J.* **27**, 588–592.

Fessas, Y. P. & Weiland, R. H. 1982 Convective solids settling induced by a buoyant phase – a new method for the acceleration of thickening. *Resources and Conservation* **9**, 87–93.

Fessas, Y. P. & Weiland, R. H. 1984 The settling of suspensions promoted by rigid buoyant particles. *Intl J. Multiphase Flow* **10**, 485–507.

Graham, W. & Lama, R. 1963 Sedimentation in inclined vessels. *Can. J. Chem. Engng* **41**, 31–32.

Greenspan, H. P. & Ungarish, M. 1982 On hindered settling of particles of different sizes. *Intl J. Multiphase Flow* **8**, 587–604.

Herbolzheimer, E. 1983 Stability of the flow during sedimentation in inclined channels. *Phys. Fluids* **26**, 2043–2054.

Herbolzheimer, E. & Acrivos, A. 1981 Enhanced sedimentation in narrow tilted channels. *J. Fluid Mech.* **108**, 485–499.

Hill, W. D., Rothfus, R. R. & Li, K. 1977 Boundary-enhanced sedimentation due to settling convection. *Intl J. Multiphase Flow* **3**, 561–583.

Kinosita, K. 1949 Sedimentation in tilted vessels. *J. Colloid Interface Sci.* **4**, 525–536.

Law, H.-S., Masliyah, J. H., MacTaggart, R. S. & Nandakumar, K. 1987 Settling of bidisperse suspension: light and heavy particles. *Chem. Engng Sci.* **42**, 1527–1538.

Lockett, M. J. & Al-Habbooby, H. M. 1973 Differential settling by size of two particle species in a liquid. *Trans. Inst. Chem. Engrs* **51**, 281–292.

Lockett, M. J. & Al-Habbooby, H. M. 1974 Relative particle velocities in two-species settling. *Powder Technol.* **10**, 67–71.

Lockett, M. J. & Bassoon, K. S. 1979 Sedimentation of binary particle mixtures. *Powder Technol.* **24**, 1–7.

Masliyah, J. H. 1979 Hindered settling in a multi-species particle system. *Chem. Engng Sci.* **34**, 1166–1168.

Mirza, S. & Richardson, J. F. 1979 Sedimentation of suspensions of particles of two or more sizes. *Chem. Engng Sci.* **34**, 447–454.

Nakamura, H. & Kuroda, K. 1937 La cause de l'acceleration de la vitesse de sedimentation des suspensions dans les recipients inclines. *Keijo J. Med.* **8**, 256–296.

Oliver, D. R. & Jenson, V. G. 1964 The inclined settling of dispersed suspensions of spherical particles in square-section tubes. *Can. J. Chem. Engng* **42**, 191–195.

Patwardhan, V. S. & Tien, C. 1985 Sedimentation and liquid fluidization of solid particles of different sizes and densities. *Chem. Engng Sci.* **40**, 1051.

Pearce, K. W. 1962 Settling in the presence of downward facing surfaces. *Proc. 3rd. Congr. Eur. Fed. Chem. Engng.* pp. 30–39.

Ponder, P. 1925 On sedimentation and rouleaux formation. *Q. J. Exp. Physiol.* **15**, 235–252.

Richardson, J. F. & Meikle, R. A. 1961 Sedimentation and fluidization part III. *Trans. Inst. Chem. Engrs* **39**, 348–356.

Schaflinger, U. 1985*a* Experiments on sedimentation beneath downward-facing inclined walls. *Intl J. Multiphase Flow* **11**, 189–199.

Schaflinger, U. 1985*b* Influence of nonuniform particle size on settling beneath downward facing walls. *Intl J. Multiphase Flow* **11**, 783–796.

Schneider, W. 1982 Kinematic-wave theory of sedimentation beneath inclined walls. *J. Fluid Mech.* **120**, 323–346.

Selim, M. S., Kothari, A. C. & Turian, R. M. 1983 Sedimentation of multisized particles in concentrated suspensions. *AIChE J.* **29**, 1029–1038.

SHANNON, P. T., DEHAAS, R. D., STROUPE, E. P. & TROY, E. M. 1964 Batch and continuous thickening. Prediction of batch settling behaviour from initial rate data with results for rigid spheres. *Indust. Engng Chem. Fund.* **3**, 250–260.

SHANNON, P. T., STROUPE, E. & TORY, E. M. 1963 Batch and continuous thickening. Basic theory. Solids flux for rigid spheres. *Indust. Engng Chem. Fund* **2**, 203–211.

SMITH, T. N. 1966 The sedimentation of particles having a dispersion of sizes. *Trans. Inst. Chem. Engrs* **44**, T153–157.

VOHRA, D. K. & GHOSH, B. 1971 Studies of sedimentation in inclined tubes. *Indust. Engng Chem.* **13**, 32–40.

WEILAND, R. H., FESSAS, Y. P. & RAMARAO, B. V. 1984 On instabilities arising during sedimentation of two-component mixtures of solids. *J. Fluid Mech.* **142**, 383–389.

WEILAND, R. H. & MCPHERSON, R. R. 1979 Accelerated Settling by Addition of Buoyant Particles. *Indust. Engng Chem. Fund* **18**, 45–49.

WHITMORE, R. L. 1955 The sedimentation of suspensions of spheres. *Brit. J. Appl. Phys.* **6**, 239–245.

ZAHAVI, E. & RUBIN, E. 1975 Settling of solid suspensions under and between inclined surfaces. *Indust. Eng. Chem. Process Des. Develop.* **14**, 34–40.